applied sciences

MDPI

Article

Estimation Method of Wind-Induced Fatigue of Metal Roof Claddings under Typhoon: Numerical Analysis and Experimental Comparison

Ying Xuan [1], Zhuangning Xie [1,*], Lele Zhang [1,2] and Qiusheng Li [3]

[1] State Key Laboratory of Subtropical Building Science, South China University of Technology, Guangzhou 510641, China; ncuxuanying@163.com (Y.X.); zhanglele19891217@163.com (L.Z.)
[2] China Construction Second Engineering Bureau Co., Ltd., South China Company, Shenzhen 518048, China
[3] Department of Civil and Architectural Engineering, City University of Hong Kong, Hong Kong; bcqsli@cityu.edu.hk
* Correspondence: znxie@scut.edu.cn

Abstract: Equivalent load cycle sequence (ELCS) is important basic information to know that affects the reliability of the evaluation of wind-induced fatigue on metal roof claddings. In this study, an estimation method of wind-induced fatigue of metal roof claddings is proposed. Based on the measured wind pressure–time history data of the roof claddings on a full-scale low-rise building located along the coast of South China during a typhoon, a new ELCS (NELCS) that reflects typhoon and actual structure wind pressure characteristics in China's coastal areas is obtained by using the rainflow counting method. The locations of fatigue hot spots of metal roof panels are analyzed by using the finite element analysis method, and the relationship between hot spot stress and wind pressure is obtained. The fatigue damage accumulation of metal roof claddings under the ELCS of a typhoon process is counted by the linear cumulative fatigue theory, commonly known as Miner's rule. The fatigue damage accumulation of roof claddings with different purlin distances and design wind loads is analyzed using this method and then compared with the results from the dynamic loading test of an air chamber. Results show that the physical test findings are close to the numerical calculation results, which proves that the numerical calculation method has high accuracy and reliability. The comparison between NELCS in this study and the Australian standard low-high-low (LHL) sequence shows that the LHL loading sequence is conservative.

Keywords: roof claddings; wind-induced fatigue; equivalent load cycle sequence; numerical analysis; wind-resistance fatigue test

check for updates

Citation: Xuan, Y.; Xie, Z.; Zhang, L.; Li, Q. Estimation Method of Wind-Induced Fatigue of Metal Roof Claddings under Typhoon: Numerical Analysis and Experimental Comparison. *Appl. Sci.* **2022**, *12*, 6785. https://doi.org/10.3390/app12136785

Academic Editors: Fernanda Rodrigues and Sergio Montelpare

Received: 28 May 2022
Accepted: 30 June 2022
Published: 4 July 2022

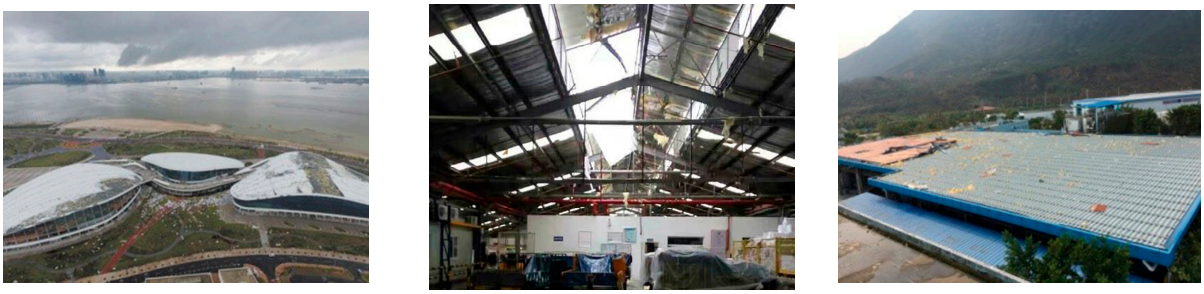
Publisher's Note: MDPI stays neutral with regard to jurisdictional claims in published maps and institutional affiliations.

Copyright: © 2022 by the authors. Licensee MDPI, Basel, Switzerland. This article is an open access article distributed under the terms and conditions of the Creative Commons Attribution (CC BY) license (https://creativecommons.org/licenses/by/4.0/).

1. Introduction

Metal roof claddings are widely used in various long-span structural enclosure systems, such as industrial buildings, gymnasiums, airport terminals, and railway stations, because of their advantages of light weight, high strength, unique shape, and flexibility. However, the stress change of roof claddings under typhoon loading may cause the accumulation of fatigue, consequently affecting usage and raising safety concerns. Emanuel [1] pointed out that the records of net power dissipation of hurricanes are highly correlated with sea surface temperature, and the tropical cyclone intensity increases as the climate warms up. Knutson et al. [2] indicated that the greenhouse effect will lead to a 2–11% increase in the average intensity of tropical cyclones by 2100, and the frequency of the strongest cyclones will increase significantly. Webster et al. [3] analyzed the number, days, and intensity of tropical cyclones under the climatic conditions of rising sea surface temperature in the past 35 years, and suggested that the number and proportion of hurricanes of category 4 and category 5 have increased significantly. Mei et al. [4] found that typhoons hitting east and southeast Asia have increased by 12–15% over the past 37 years, and

that the annual incidence of category 4 and category 5 typhoons has more than doubled. Li et al. [5] found that the tropical cyclones that make landfall in China have become more destructive in recent decades. Typhoon No. 22 Mujigae landed in Zhanjiang in 2015, causing serious damage to space-enclosing structures of several of Baosteel's projects that were under construction, in addition to the roofs of several venues of Zhanjiang Olympic Sports Center (Figure 1a). Typhoon Meranti landed in Xiamen in 2016, causing serious damage to the Xiamen hangar (Figure 1b). In 2017, Typhoon No. 13 Hato landed in Zhuhai and destroyed a large number of metal roofs (Figure 1c). The analysis and detection of anti-fatigue effects of metal roof claddings under fluctuating wind load of typhoons are important factors in the wind-resistance design of long-span metal roof systems. Typhoon equivalent load cycle sequence (ELCS) is important basic information required for the wind-induced fatigue evaluation of metal roof claddings.



(**a**) (**b**) (**c**)

Figure 1. Typhoon-induced failure of metal roof: (**a**) roof damage of Olympic Sports Center Stadium in Zhanjiang; (**b**) wind-related disaster of hangar roof of Xiamen Airport; (**c**) wind-related disaster on roof system in Zhuhai.

Tropical cyclone Tracy destroyed a great number of roof claddings in 1974. Therefore, it is necessary to develop a typhoon equivalent loading sequence in order to verify the fatigue strength of roof claddings. The standard fatigue test sequence of DABM [6] adopts 10,000 cycles with the design wind load as the standard amplitude. However, the constant amplitude cycle of this sequence does not reflect the wind load distribution characteristics of tropical cyclones. Melbourne [7] defines the ELCS according to the hourly mean pressure and the rms of the pressure fluctuations, which is equivalent to the 1-hour random wind load under the maximum design wind speed in the 50-year return period. The equivalent load sequence of 5000 cycles per hour is recommended to be repeated three times in order to simulate the load of tropical cyclones. Jancauskas et al. [8] researched the fatigue characteristics of a corrugated metal roof under the action of a simulated tropical cyclone by combining the wind tunnel pressure and cyclic load tests, counting the damage accumulation of metal roof claddings, and comparing the calculated results with the results of low and high three-level loading sequence tests of TR440 [9]. Mahendran [10,11] summarized the wind-induced damages of low-rise buildings in Australia for years, and proposed that the roof panels are often damaged under the action of strong winds; this resulted from insufficient strength of the joint parts or from wind-induced fatigue. The author further reviewed the fatigue loading sequences of various countries. Based on the wind tunnel test pressure data of a typical house model and the wind speed and direction data of a typical simulated cyclone, the LHL four-level load cycle sequence is proposed to simulate the action of a cyclone, which is the ELCS closest to the actual situation in existing fatigue testing sequences. The current fatigue design of metal roof in Australian cyclonic regions is based on the LHL loading sequence specified in the National Construction Code [12]. Wu et al. [13] used ABAQUS software to analyze the damage of the finite element model of aluminum alloy roofing system standard specimens under the action of eight load sequences in the load cycle, as recommended by CSA. According to the damage results obtained from numerical analysis, a simplified load sequence based on a CSA-recommended load cycle was proposed.

The wind resistance performances of metal roof systems are complex. Henderson et al. [14,15] studied the low-cycle fatigue response of a corrugated metal roof cladding by subjecting cladding specimens to a series of static, cyclic, and simulated tropical cyclone loadings. They pointed out that the peak value of cyclic loading and the corresponding amplitudes are the main determinants of the generation and development of fatigue cracks. When the cyclic loads exceed the local plastic deformation load of cladding, the number of cycles to failure is significantly reduced. Lovisa et al. [16] investigated the mechanism of fatigue crack initiation in roof cladding, and established a fatigue crack initiation criterion based on strain. Myuran et al. [17–19] investigated the fatigue performance of metal roof batten to purlin screw fastener connections, and proposed fatigue design equations for crack initiation and complete failure of roof batten to purlin connections. Sivapathasundaram et al. [20,21] studied roof battens' pull-through capacity by using experimental methods and numerical analysis; they provided design criterion and capacity reduction factors for the pull-through capacities calculation of roof battens. Lu et al. [22] used experimentation and simulations to analyze the wind-resistance performance and failure pattern of the 360° vertical seam-locked metal roof system, and proposed a method to improve the wind resistance of metal roof systems.

It is important to analyze and predict wind-induced damage for long-span roofs. Rocha et al. [23] used a numerical analysis model and measured wind pressure–time history to evaluate the reliability of roof panels exposed to a specific hurricane event. They proposed that finite element analysis can be simplified by using a series of sequential linear–elastic static analyses. Ji et al. [24] proposed a probability analysis method for wind-induced damage of metal roof claddings based on wind tunnel test data, and used the Copula function to study the influence of wind load correlation on roof damages. Huang et al. [25] proposed a wind-induced damage estimation method of roof claddings by considering the correlation of roof wind load, and pointed out that ignoring the correlation of wind load will underestimate the risk of roof cladding damage. Huang et al. [26] studied the wind-induced fatigue failures of long-span lattice structures. They used numerical methods to estimate the fatigue damage to the grid and spherical joints in the steel lattice structure, considering the joint distribution of wind speed and direction, and based on wind tunnel pressure test data and the fatigue accumulation theory.

At present, the ELCS closest to actual situations uses only the roof wind pressure–time history data obtained by analyzing the wind tunnel pressure test data, and through simulated typhoon wind speed and direction data. Given the differences between the model tests and the full-scale prototype measured results and the regional differences of typhoons, a gap exists between these simulated data and the wind pressure distribution of the actual full-scale roof structure under the action of actual typhoons. Therefore, the existing typhoon ELCS cannot be fully applicable to typhoon-prone areas in the southeast coast of China.

This study proposes a new ELCS (NELCS) that conforms to the typhoon characteristics in the southeast coast of China and reflects the wind pressure distribution characteristics of actual structures based on the measured data of wind pressure–time history of a typical typhoon in the southeast coast of China. Based on this sequence, the estimation method of wind-induced fatigue damage to metal roofs is established by using finite element analysis and Miner's linear cumulative fatigue theory. This study used YX35-760 self-drilling screw-fastened metal roof claddings as examples to estimate the fatigue damage degree of roof claddings with different purlin distances and design wind loads. Subsequently, the measured wind pressure–time history and LHL sequence are compared. The dynamic loading test of an air chamber under the same working condition is carried out in order to check the results of the numerical analysis, and the differences between numerical simulation and physical test results are analyzed. The YX35-760 self-drilling screw-fastened metal roof claddings test specimens were produced by Chess Lab in Zhuhai, China.

2. Fatigue Analysis Methods

The relationship between load and fatigue life needs to be established in order to estimate the fatigue life of materials or structures. The relationship curve between the cyclic load and its corresponding number of cycles to failure obtained through the fatigue test is called the *S*–*N* curve, as shown in Figure 2, which is given as follows:

$$NS^m = K, \tag{1}$$

where N is the number of cycles to failure for stress amplitude S; and m and K are material parameters to be determined. Then, the logarithms on both sides of Equation (1) are taken as follows, in order to obtain the *S*–*N* curve in logarithmic form:

$$\lg N = a + b \cdot \lg S, \tag{2}$$

where a and b are constants to be determined, which are taken from reference [27].

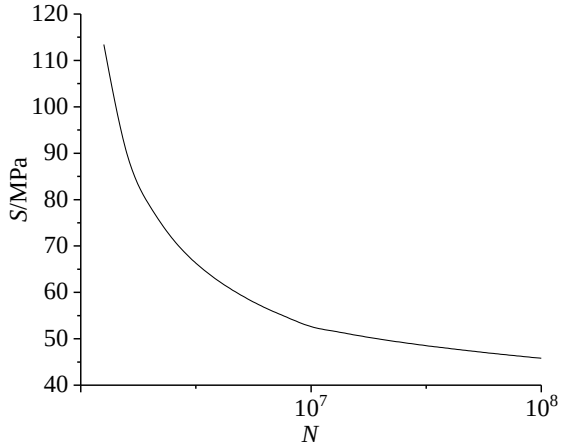


Figure 2. *S*–*N* curve of the materials.

The stresses used for fatigue analysis are classified as nominal stresses and hot spot stresses. The nominal stresses in a component can be derived by using classical theories. If the positions for fatigue analysis are located in the stress concentration area caused by the global shape of the structure, the stress concentration factors of the global geometric shape must be considered. Therefore, the local stresses of the positions for fatigue analysis are given as follows:

$$\sigma_{local} = SCF\sigma_{nominal}, \tag{3}$$

where *SCF* stands for stress concentration factor.

The hot spot stresses are the geometric stresses generated in consideration of the details of components. Generally, local hot spot stresses can be calculated by using a detailed structure or component model that is established by using finite element software and choosing reasonable boundary conditions; hot spot stress is obtained through loading analysis for fatigue calculation.

According to the assumption of linear cumulative damage, the amount of accumulated damage at a given level of stress is proportional to the number of cycles; this means that the fatigue damage of a material or structure is determined by a relation of the proportional damage (cycle ratio n_i/N_i) at various load levels (multi-level loading). The fatigue damage under variable-amplitude repeated loads could be predicted by the following equation [28]:

$$D = \sum_{i=1}^{k} D_i = \sum_{i=1}^{k} \frac{n_i}{N_i}, \tag{4}$$

according to Equation (1), where n_i is the number of cycles with amplitude S_i, and N_i is the number of cycles to failure for stress amplitude S_i. When $D = 1$, fatigue failure will take place.

The S–N curve is obtained from fatigue tests when the mean value of stress cycle $S_m = 0$. The mean stress value also affects the cumulative fatigue damage. When the mean stress $S_m < 0$, the fatigue life increases; when $S_m > 0$, the fatigue life decreases. Given that the mean value S_m is typically non-zero, the following Goodman method is used to provide an equivalent stress amplitude with zero mean level:

$$S_a = S_{-1}(1 - \frac{S_m}{S_u}), \tag{5}$$

where S_a is the stress amplitude at non-zero mean value, S_{-1} is the stress amplitude at the zero-mean value, S_m is the average stress, and S_u is the tensile strength of the material.

The rainflow counting method [29] is widely used in the study of structural fatigue performance. The stress–time or load–time history is counted, one by one, and divided into independent cycles in order to calculate the fatigue life, or to compile the load spectrum of fatigue tests. The occurrence times of each stress amplitude and their corresponding average stresses under a certain stress–time history can be obtained by using this method. After all stress amplitudes and stress mean values are counted, the equivalent stress amplitudes are provided by the Goodman method. Then, the accumulated fatigue damage under a certain stress–time history can be obtained by using the material S–N curve and linear cumulative fatigue theory.

3. NELCS of a Typhoon

During the typhoon field measurement process, the external pressures on the roof of the moveable instrumented building are monitored by using the wind pressure transducers, and the 3D wind velocity information provided by anemometers. Typhoon Chanthu (201003) was generated in the sea area about 900 km south-southeast of Hong Kong on 19 July 2010 and moved northwest. On 20 July, Chanthu intensified into a tropical storm and moved westwards for a while during that night. Chanthu intensified into a severe tropical storm on 21 July. Then, Chanthu resumed a northwesterly track and intensified into a typhoon. At 13:45 on 22 July, Chanthu landed near Wuchuan City, Guangdong Province, and weakened into a severe tropical storm.

The moveable instrumented building was located on the seashore near Diancheng Town, Wuchuan City, at latitude 20°40′ N and longitude 111°30′ E. The instrumented building is 6 m × 4 m × 4 m. A drainage gradient of 2% was set on the flat roof. Wind pressure transducers were installed on the roof of the instrumented building. A 10-meter meteorological tower was located 7 m away from the building. Three RM young anemometers were mounted on the tower at heights of 4, 7.5, and 10 m from the ground. Moreover, a Wind Master Pro 3D ultrasonic anemometer (UK Gill Instruments, Lymington, UK) was installed at a height of 10 m on the tower. The locations of pressure taps on the roof of the building are shown in Figure 3 [30].

The ultrasonic anemometer measurement at the height of 10 m shows that the maximum 3-second gust wind speed of typhoon Chanthu was 41.4 m/s, and the maximum 10-minute mean wind speed was 30.3 m/s. Tap12 located at the windward leading edge on the corner was consistently subjected to the most severe suction pressures for quartering winds; the peak suction pressure recorded during the typhoon was −4.24 kPa. The pressures during the strongest storm from 8:00 to 13:00 are shown in Figure 4.

The pressure records were counted and analyzed by using the rainflow method. Each cycle in the pressure record was sorted according to its mean value and range. The pressure ranges and mean values were simplified and divided into 10 levels to form a 10 × 10 matrix. The number of cycles of each cell was counted, as shown in Figure 5. The matrix is composed of the cycles of the combinations of different wind pressure range cells

and mean value cells. The range cells and mean cells are displayed in the ratio to the peak suction pressure recorded during the typhoon.

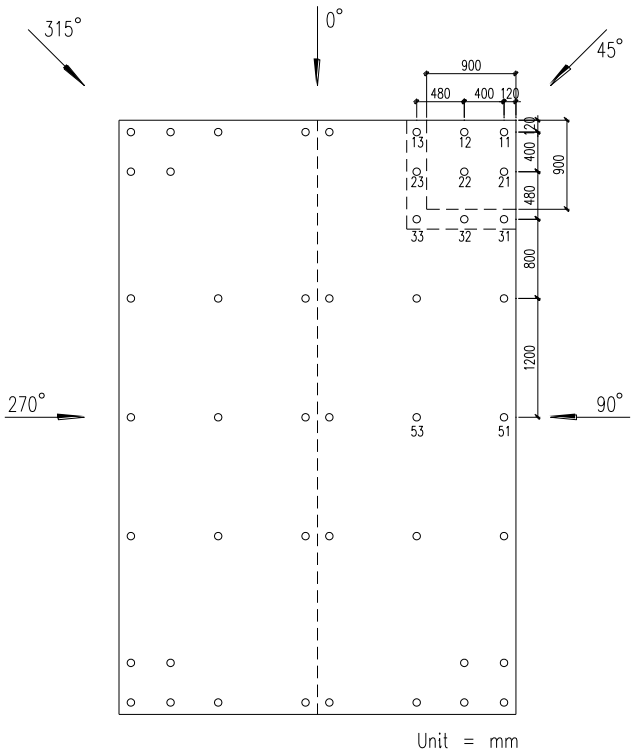


Figure 3. Locations of pressure taps.

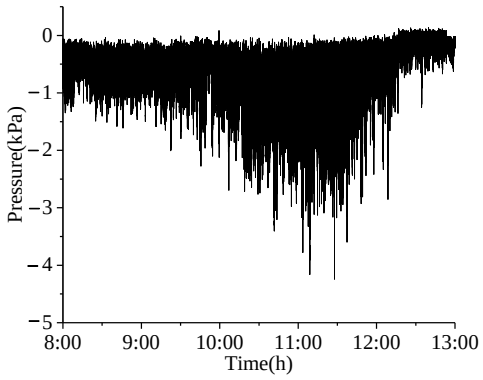


Figure 4. Time history of pressures from 8:00 to 13:00.

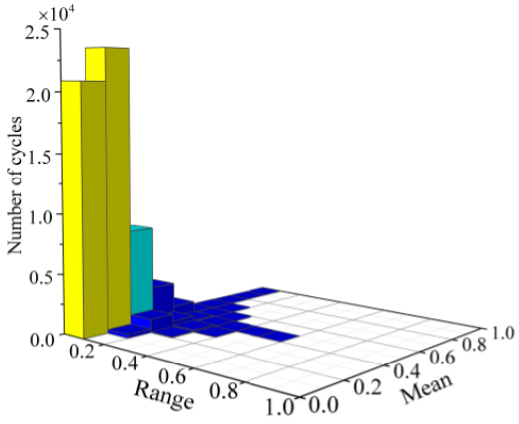


Figure 5. Wind loading rainflow matrix.

After the rainflow statistics and simplification division, the wind loading matrix is still complex and is not acceptable for use in an engineering test. Accordingly, the matrix still needs to be further simplified. Mahendran [11] researched the fatigue behavior of metal roof claddings and pointed out that the maximum load and the range have a more significant influence on the fatigue performance of metal roof claddings than the mean value. Twenty-four non-zero loading cells represent the pressure records during the typhoon in Figure 5. The ratio of the average maximum load of each cell to the peak suction pressure during the typhoon is defined as the load ratio, and the corresponding cycle times are counted according to the load ratio of each cell. Then, the 24 non-zero cells were further simplified into a four-level loading sequence with a zero minimum load and a maximum load of 0.4, 0.6, 0.8, and 1.0 times the ultimate design load. All the cells of loading in Figure 5 with a load ratio of between 0 and 0.4 were allocated to the four-level loading sequence with a load ratio of 0–0.4. The loading cells with a load ratio of between 0.4 and 0.6 were allocated to the loading sequence with a load ratio of 0–0.6. Meanwhile, the loading cells with a load ratio of between 0.6 and 0.8 were allocated to the loading sequence with a load ratio of 0–0.8. Furthermore, the loading cells with a load ratio of between 0.8 and 1.0 were allocated to the loading sequence with a load ratio of 0–1.0. The four-level loading sequence is similar to the distribution characteristics of non-zero loading cells in Figure 5.

The linear damage model is used based on the assumption that the damage generated by a single cycle of variable amplitude load can be calculated by the fatigue-life equation and Miner's rule. The damage caused by a single cycle constituting the wind loading time history is assumed to linearly accumulate. Different cycles are independent of each other and do not delay or accelerate the damage accumulation. According to Equation (1), the fatigue equivalent calculation rule for a similar level is:

$$N_s = N_t(S_t/S_s)^m, \tag{6}$$

where S_s is the stress amplitude of the loading cell in the four-level loading sequence; S_t is the stress amplitude of each loading cell in the typhoon matrix; m is the parameter of the fatigue life curve; and N_t and N_s are the cycles to fatigue failure corresponding to S_t and S_s, respectively. The fatigue life equation will not be the same for different roof claddings. Mahendran [11] pointed out that the value of m is generally two or three, and the value of m is one for the typhoon ELCS. The number of equivalent cycles for each cell was carried out according to Equation (5). Then, the number of cycles at the same load level was accumulated. The typhoon equivalent load sequence is further simplified according to the above method, as shown in Table 1.

Table 1. ELCS of typhoon.

Stage	Cycles	Load
A	4000	0–0.4 *P*
B	300	0–0.6 *P*
C	25	0–0.8 *P*
D	3	0–1.0 *P*
E	25	0–0.8 *P*
F	300	0–0.6 *P*
G	4000	0–0.4 *P*

P indicates the test wind loading, which is obtained by multiplying the design wind loading with the corresponding assurance coefficients.

4. Fatigue Damage Analysis

4.1. Finite Element Analysis

The locations of fatigue hot spots of metal roof claddings under wind load were analyzed by the finite element method, and the relationship between hot spot stress and

wind pressure was obtained. This study used YX35-760 self-drilling screw-fastened metal roof cladding as an example to introduce the stress analysis process of metal roof cladding under wind loading.

4.1.1. Model Establishment and Loading

Xu [31] suggested that the wind load resistance performance of a profiled metal roof can be studied through two-span roof panels. Moreover, Xu [32] pointed out that when the roof is large, the lap joints between the roof panels have little effect on its wind resistance performance, and the roof can be treated as an infinite continuous plate. Henderson [14] proposed that the wind resistance behavior of a profiled roof panel system can simulate the effect of wind load by uniformly distributed pressure.

Finite element software ANSYS 14.5 was used to establish a one-span model with YX35-760 self-drilling screw-fastened metal roof claddings as the prototypes. The dimensions of the roof panel are shown in Figure 6. The material parameters of the roof panel are shown in Table 2 according to the tensile test results of the specimens, and the graded loading method was adopted for finite element analysis.

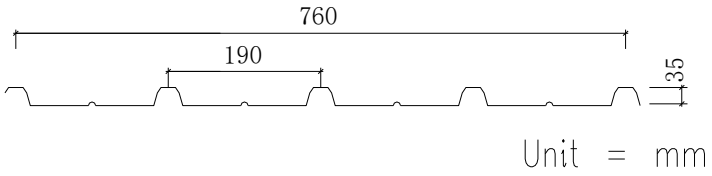


Figure 6. Dimensions of the YX35-760 metal roof panels.

Table 2. Material information of roof panels.

Cladding Thickness (mm)	Young's Modulus (GPa)	Poisson's Ratio	Yield Strength (MPa)	Tangent Modulus (MPa)
0.426	205	0.3	349	4100

In the finite element model, the metal roof panel selects the shell181 element. Meanwhile, the washer and screw head select the solid185 element. The metal roof panel material is assumed to be a type of perfectly elastic plastic material, and the bilinear model was adopted. The rubber washer adopts the Mooney–Rivlin model. The parameters were set referring to document [33].

A fine mesh was used in the vicinity of the fastener hole. The contacts between the washer and the roof panel and between the washer and the screw heads were bonded. Given that the roof claddings were screw-fastened at each crest, symmetry conditions were assumed along each crest. Figure 7 shows the boundary conditions used.

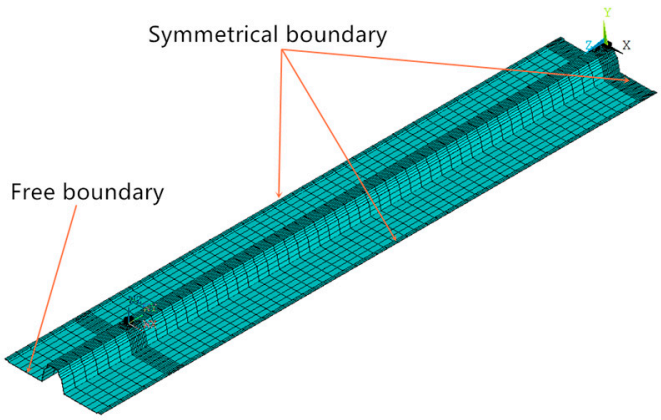


Figure 7. Boundary condition setting.

4.1.2. Load–Stress Relationship

The analysis results show that the element nodes close to fastener holes bear heavier stress. The element stress values near the fastener holes were obtained by post-processing. The nodes with the most severe stresses near the fastener holes were selected as the fatigue hot spots. The von Mises equivalent stress was used to calculate the fatigue damage accumulation. Figure 8 shows the stress distribution of the finite element model when the purlin distance is 600 mm. The subsequent fatigue analysis adopted the hot spot stress for the calculation.

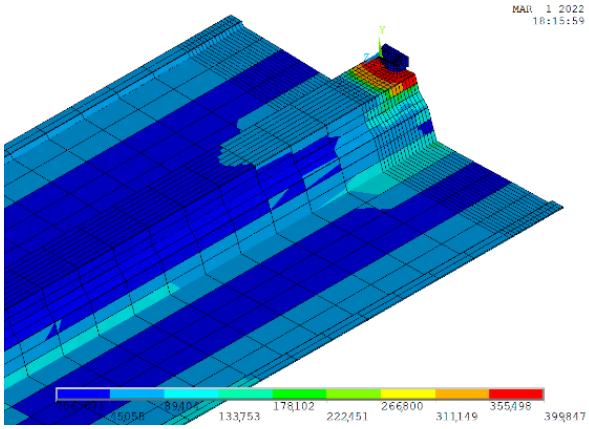


Figure 8. Stress distribution of the finite element model when the purlin distance is 600 mm.

Nine groups of finite element models with a purlin distance from 600 mm to 1000 mm were established. After loading and analysis, the relationships between hot spot stress and pressure of different purlin distance models are obtained, as shown in Figure 9. The hot spot stress of nine groups of finite element models increases with an increase in purlin distance. With graded loading, the hot spot stress of each model increases gradually in the bilinear model.

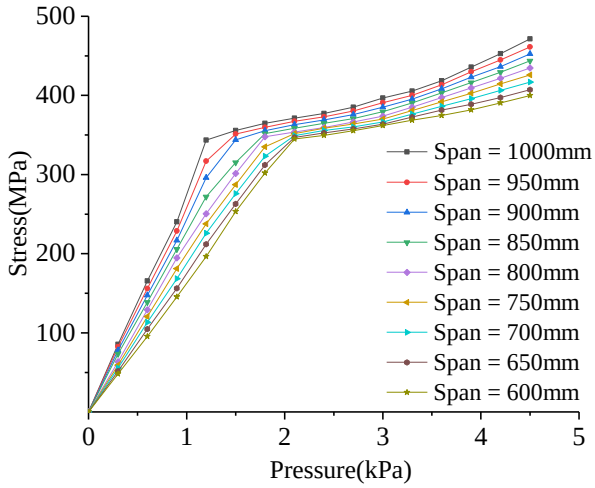


Figure 9. Load–stress relationship of different purlin distances.

4.2. Fatigue Damage Statistics

The purlin distances of roof claddings were set from 600 to 1000 mm (600, 800, and 1000). When the stress time history of Typhoon Chantu was loaded, the hot spot stress time history of roof claddings was calculated according to the pressure records during the typhoon and the finite element analysis results. The stress time history was counted and analyzed using the rainflow statistics method. When the NELCS and the LHL sequence were loaded on the roof claddings, the wind loading P is the maximum value of the pressure

record during the typhoon (4.24 kPa). The hot spot stress cycles were obtained based on finite element analysis results. Then, the fatigue damage accumulation of the roof claddings was counted in combination with the material *S–N* curve, the Goodman formula, and Miner's linear damage accumulation rule. The fatigue damage calculation results are shown in Table 3.

Table 3. Statistical results of roof fatigue damage.

Load Mode \ Purlin Distance (mm)	600	800	1000
Typhoon Chantu	0.009	0.167	0.643
NELCS	0.076	0.504	1.193
LHL	0.269	0.706	1.972

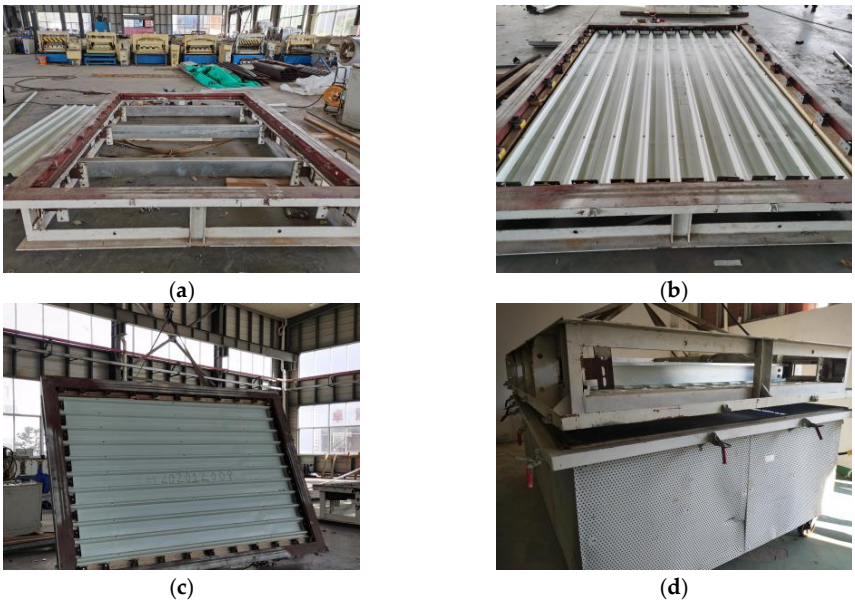
In Table 3, the fatigue damage accumulation obtained by loading the LHL sequence is more conservative compared with the fatigue damage calculation results based on the Typhoon Chantu pressure record. The results of NELCS in this study fall between the preceding two methods. Therefore, our results are more reasonable because NELCS not only considers the safety, but it is also not too conservative.

5. Wind Fatigue Tests

In order to verify the effectiveness of the above-mentioned methods, dynamic air chamber tests were carried out for the actual segment metal roof system to investigate the fatigue damage of roof panels with different purlin distances and design wind loads of NELCS. The test outcomes were compared with the corresponding numerical simulation analysis results.

5.1. Test Equipment and Installation

The test equipment used included a test chamber, wind pressure supply devices, and pressure measurement and control devices. The plan view size of the test chamber was 3070 mm × 2130 mm. The testing instrument was a KFJC-006 flow wind resistance test machine, which belongs to Chess Lab in Zhuhai, China. The experimental setup is shown in Figure 10.



(**a**) (**b**) (**c**) (**d**)

Figure 10. Experimental setup: (**a**) purlin installation; (**b**) roof panel installation; (**c**) lifting; (**d**) installed apparatus in the test chamber.

The specimen YX35-760 self-drilling screw roof claddings were installed in the test chamber. The roof claddings were galvanized profiled steel panels. The material parameters are shown in Table 2. ST5.5 × 65 hexagon self-drilling screws with washers were used as the fasteners. The purlin is C150 × 65 × 13 × 2.0. The purlin distances were set as 600, 800, and 1000 mm, in order to consider the influence of purlin distance. The layouts of the roof test specimens and the screw arrangement are shown in Figure 11.

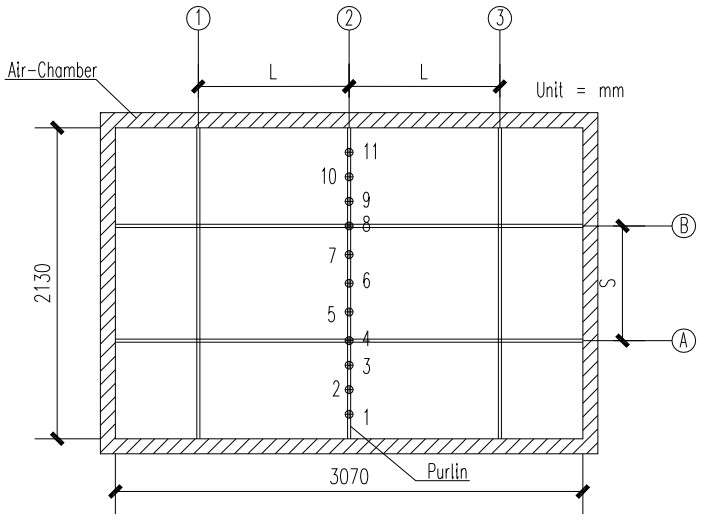


Figure 11. Test observation screw arrangement. The number is the screw arrangement, L is purlin distance, S is the width of a roof panel.

5.2. Test Loading

The dynamic wind load cycle to simulate the effect of wind gusts was set to 3 s. Table 1 provides the detailed load methods. In this way, the fatigue properties of the metal roof specimens under the action of dynamic cyclic wind pressure were tested. Figure 12 is the NELCS.

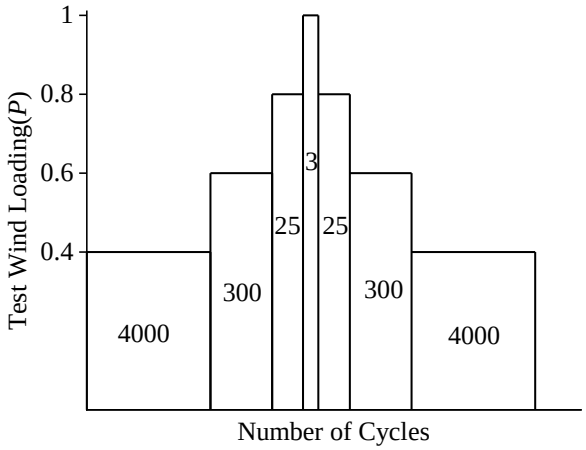


Figure 12. New equivalent load cycle sequence (NELCS).

(1) A dynamic pressurization cycle includes pressure rise and fall. The pressure rise time shall be less than or equal to 2 s; the fall time shall be less than or equal to 1 s; the single fluctuation cycle shall be less than or equal to 3 s.
(2) The dynamic wind pressure test is based on the design wind pressure *P*.
(3) According to Table 1, the tests of each stage are completed in sequence from stage A until the roof panel specimens are cracked, or when three rounds of dynamic loading are completed.

According to the 3-second loading cycle, the sequence loading defined in Table 1 takes about 7 h to complete.

5.3. Test Parameters and Results

Two groups of test parameters were used for the tests. In group A, the purlin distance was 1000 mm, and the design wind pressures were 4.5, 3.6 (repeated twice), and 3.0 kPa (repeated twice). In the other group, the design wind pressure was 4.5 kPa, and the purlin distances were 600 and 800 mm. Seven working conditions were included in the two groups. The failure stages of the two groups of test results are summarized in Table 4.

Table 4. Summary of the test results.

Group	*P* /kPa	Span /mm	Failure Stage	Damage Estimation
I	3.0	1000	Stage B of the second round of loading	0.67–1.0
	3.0		Stage C of the second round of loading	0.67–1.0
	3.6		Mid-stage G of the first round of loading	1.0–1.3
	3.6		End-stage G of the first round of loading	1.0
	4.5		Stage F of the first round of loading	1.0–2.0
II	4.5	800	End-stage G of the first round of loading	1.0
		600	No damage observed in the three rounds of test	0–0.33

The effects of different wind pressures and purlin distances on the fatigue damage of metal roof claddings were observed in the tests. The wind-induced fatigue failure processes of metal roof panel were divided into four stages according to the observation and records of the test processes. First, the fastener holes of the roof specimen became larger due to reciprocating cyclic loading, thus complete and effective constraints are impossible to form. Obvious uplift deformations near the fastener holes were observed with continuous loading. Then, the locations with maximum deformations developed into cracks. When cyclic loading was continued, multiple cracks were generated near the fastener holes, which gradually deepened and merged to form cracks with the loading process. The failure process is shown in Figure 13.

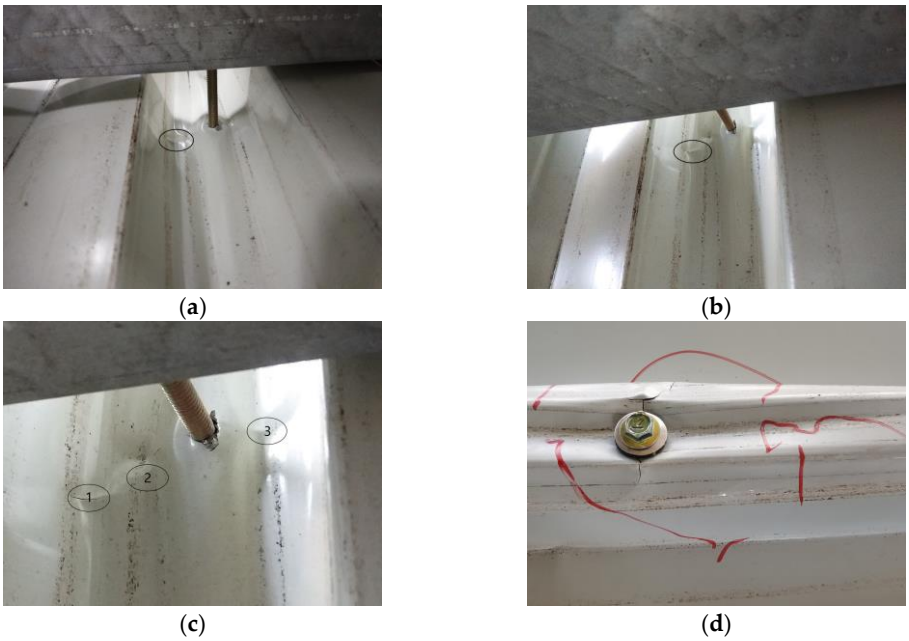


Figure 13. Wind-induced fatigue failure process of metal roof: (**a**) uplift deformation; (**b**) rack generation; (**c**) three cracks; (**d**) cut-through cracks.

The damage estimation in Table 4 was obtained based on the estimated results according to the cycle stage of roof failure. When P = 3.0 kPa in the group I working condition with a purlin distance of 1000 mm, two tests showed that fatigue cracks appeared on the roof panes in stages B and C of the second round of loading. There was no fatigue failure in the first round of loading. It could be concluded that the damage value of single round loading was less than 1. In the second round of loading, fatigue failure occurred before half of the loading was completed. Therefore, the single round loading damage was greater than 1/1.5, which means that the damage for a single round loading ranges between 0.67 and 1. When P = 3.6 kPa, the fatigue cracks of the roof panels in the two tests occurred in the middle and end of stage G of the first round of loading. Fatigue failure occurred before the first round of loading was completed. As a result, the damage value of single-round loading was considered to be greater than 1. The damage caused by each loading cycle in stages B–F is greater than that in the A and G stages. If the single loading cycle damage in stages B–F is divided into two parts, one of them is defined as D, which is equal to the single loading cycle damage value in stage A and G. The sum of the remaining damage in the B–F loading stages is defined as D_{others}. Then, the cumulative damage in the process of one round of loading is 8653 D + D_{others}, since fatigue failures occurred in the middle and late G stage of the two tests. The most unfavorable result of the two tests is 6653 D + D_{others}, thus it is considered that the damage value of single-round loading (8653 D + D_{others})/(6653 D + D_{others}) is less than 1.3. Therefore, the fatigue damage of the first round was about 1.0 to 1.3. When P = 4.5 kPa, the fatigue cracks of roof panel appeared in the F stage of the first round of loading. In the first round of loading, fatigue failure occurs after the loading is half-completed but not fully, and its single round fatigue damage could be estimated to be approximately between 1.0 and 2.0. When P = 4.5 kPa in the group II working condition, the influences of different purlin distances were considered. When the purlin distance was 800 mm, the fatigue crack of the roof panel appeared near the end of stage G of the first round of loading, and the single-round fatigue damage could be estimated to be about 1.0. When the purlin distance was shortened to 600 mm, the roof panel did not fail even after three rounds of loading. Therefore, the fatigue damage of roof panels under single-round loading was not greater than 0.33; that is, the damage range was 0 to 0.33.

5.4. Comparison between Numerical Analysis and Experimental Results

The corresponding numerical analysis is carried out for the two working conditions in Table 4 and compared with the test results, as shown in Figure 14. The trend of the numerical analysis results is consistent with the test results. The value is slightly smaller than the test results because the initial defects in the production and installation of the roof panels were not considered in the establishment of the numerical model.

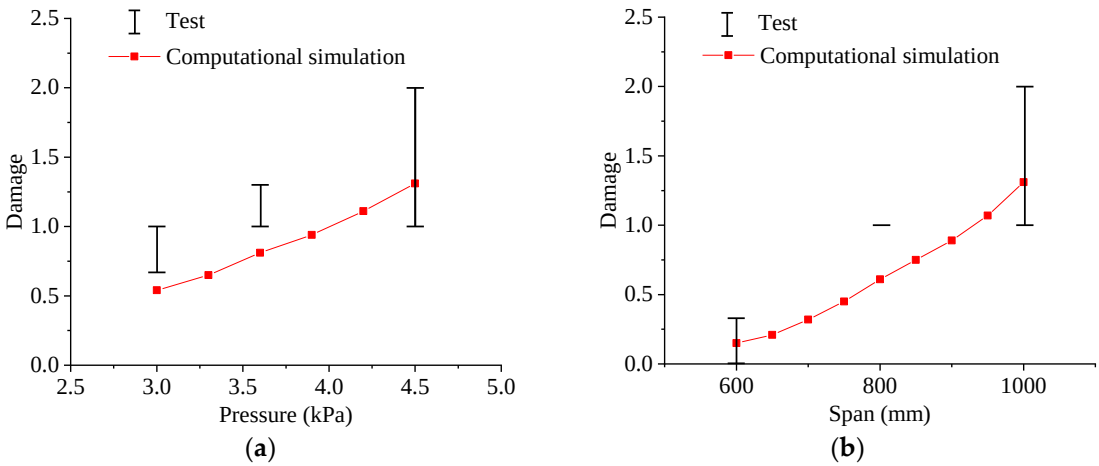


Figure 14. Comparison between numerical analysis and test results of roof damage: (**a**) influence of wind pressure; (**b**) influence of purlin distance.

The following formula is used to measure the differences between the two methods:

$$\varepsilon = 1 - \frac{Simulated\ damage\ value}{Test\ damage\ value}. \quad (7)$$

When the design wind pressures were 3.0, 3.6, and 4.5 kPa in the group I working conditions, the corresponding fatigue damage obtained from the numerical analysis were 0.54, 0.81, and 1.31, as shown in Figure 14a. According to Table 4, the ranges of ε values under these three loads were 19–46%, 19–38%, and −31–34.5%, respectively. The last group of numbers are the positive and negative deviations, which indicate the effectiveness of the numerical simulation method by comparing the simulated values and the range of the test values. Most deviation values are positive, and the maximum value is 46%. This notion means that up to 46% of damage could be underestimated by the numerical analysis. According to Table 3, the damage value of NELCS loaded in this study is much more conservative than that directly loaded by the actual wind pressure–time history. This study considers that this 46% deviation is acceptable.

The influence of purlin distance on roof damage value was investigated when the design value of wind pressure was 4.5 kPa. When the roof purlin distance was shortened from 1000 mm to 800 and 600 mm, the fatigue damage could be reduced from 1.31 to 0.61 and 0.15 by numerical simulation analysis, respectively, as shown in Figure 14b. The damage of the roof panels can be effectively reduced, and the wind resistance of the whole roof system can be improved by shortening the purlin distance.

6. Conclusions

(1) The damage results of the metal roof claddings calculated by the equivalent load sequence proposed in this study are between the results calculated by using the measured wind pressure–time history and the LHL equivalent load sequence, which avoids being too conservative on the premise of ensuring the necessary safety.
(2) The fatigue tests under multiple working conditions were carried out through the dynamic loading test of an air chamber. The ranges of ε values under these three loads were 19–46%, 19–38%, and −31–34.5%. The test results are close to the numerical calculation results, which proves that numerical calculation has high accuracy.
(3) The purlin distance has a great influence on the degree of fatigue damage. When the design wind load is 4.5 kPa, numerical analysis results show that the fatigue damage can be reduced from 1.31 to 0.61 and 0.15 when the span of roof purlin is shortened from 1000 mm to 800 mm and 600 mm, respectively. The fatigue resistance of the roof metal roof claddings can be effectively improved, and the risk of wind damage to metal roof claddings can be reduced by properly reducing the purlin distance.

Author Contributions: Conceptualization, Y.X. and Z.X.; methodology, Y.X. and Z.X.; software, Y.X.; validation, Y.X.; formal analysis, Y.X.; investigation, Y.X. and Z.X.; resources, Z.X. and Q.L.; data curation, Y.X.; writing—original draft preparation, Y.X. and Z.X.; writing—review and editing, Y.X., Z.X. and L.Z.; supervision, Z.X.; project administration, Z.X.; funding acquisition, Z.X. All authors have read and agreed to the published version of the manuscript.

Funding: This research was funded by National Natural Science Foundation of China [grant number 51778243].

Institutional Review Board Statement: Not applicable.

Informed Consent Statement: Not applicable.

Data Availability Statement: Not applicable.

Acknowledgments: The financial support is gratefully acknowledged.

Conflicts of Interest: The authors declare no conflict of interest.

References

1. Emanuel, K. Increasing Destructiveness of Tropical Cyclones over the Past 30 Years. *Nature* **2005**, *436*, 686–688. [CrossRef]
2. Knutson, T.R.; Mcbride, J.L.; Chan, J.; Emanuel, K.; Holland, G.; Landsea, C.; Held, I.; Kossin, J.P.; Srivastava, A.K.; Sugi, M. Tropical Cyclones and Climate Change. *Nat. Geosci.* **2010**, *3*, 157–163. [CrossRef]
3. Webster, P.J.; Holland, G.J.; Curry, J.A.; Chang, H.R. Changes in Tropical Cyclone Number, Duration, and Intensity in a Warming Environment. *Science* **2005**, *309*, 1844–1846. [CrossRef]
4. Mei, W.; Xie, S. Intensification of Landfalling Typhoons over the Northwest Pacific since the Late 1970s. *Nat. Geosci.* **2016**, *9*, 753–757. [CrossRef]
5. Li, C.Y.; Zhou, W.; Shun, C.M.; Lee, T.C. Change in Destructiveness of Landfalling Tropical Cyclones over China in Recent Decades. *J. Clim.* **2017**, *30*, 3367–3379. [CrossRef]
6. Holmes, J.D.; Mullins, P.J. *Darwin Area Building Manual*; Darwin Reconstruction Commission: Darwin, The Northern Territory: Darwin, Australia, 1976.
7. Melbourne, W.H. Loading cycles for simulation of wind loading. In *Proceeding Workshop on Guidelines for Cyclone Product Testing and Evaluation*; Experimental Building Station: Sydney, Australia, 1977.
8. Jancauskas, E.D.; Mahendran, M.; Walker, G.R. Computer Simulation of the Fatigue Behaviour of Roof Cladding During the Passage of a Tropical Cyclone. *J. Wind. Eng. Ind. Aerod.* **1994**, *51*, 215–227. [CrossRef]
9. Guidelines for the Testing and Evaluation of Products for Cyclone-Prone Areas. In *Technical Record 440*; Experimental Building Station: Sydney, Australia, 1978.
10. Mahendran, M. Wind-Resistant Low-Rise Buildings in the Tropics. *J. Perform. Constr. Fac.* **1995**, *9*, 330–346. [CrossRef]
11. Mahendran, M. Towards an Appropriate Fatigue Loading Sequence for Roof Claddings in Cyclone Prone Areas. *Eng. Struct.* **1995**, *17*, 476–484. [CrossRef]
12. Australian Building Codes Board. *National Construction Code (NCC)*; Council of Australian Governments: Canberra, Australia, 2016.
13. Wu, T.; Sun, Y.; Cao, Z.; Chen, Y. A New Recommended Load Cycle for Dynamic Wind-Resistant Test of Roof System Based on the Principle of Damage Equivalence. *J. Build. Eng.* **2022**, *48*, 103911. [CrossRef]
14. Henderson, D.J.; Ginger, J.D. Response of Pierced Fixed Corrugated Steel Roofing Systems Subjected to Wind Loads. *Eng. Struct.* **2011**, *33*, 3290–3298. [CrossRef]
15. Henderson, D.J.; Ginger, J.D.; Kopp, G.A. Wind Induced Fatigue of Metal Roof Cladding During Severe Tropical Cyclones. *Struct. Congr.* **2010**, *2010*, 1205–1216.
16. Lovisa, A.C.; Henderson, D.J.; Ginger, J.D.; Walker, G. Characterising Fatigue Macrocrack Initiation in Profiled Steel Roof Cladding. *Eng. Struct.* **2016**, *125*, 364–373. [CrossRef]
17. Myuran, K.; Mahendran, M. Unified Static-Fatigue Pull-through Capacity Equations for Cold-Formed Steel Roof Battens. *J. Constr. Steel. Res.* **2017**, *139*, 135–148. [CrossRef]
18. Myuran, K.; Mahendran, M.; Sivapathasundaram, M. Pull-through Capacities of Cold-Formed Steel Roof Battens Considering Loading Rate Sensitivity. *Eng. Struct.* **2018**, *177*, 459–472. [CrossRef]
19. Myuran, K.; Mahendran, M. Fatigue Damage Models for Steel Roof Battens Subject to Variable Amplitude Cyclic Wind Suction Loading. *Thin. Wall. Struct.* **2019**, *137*, 392–410. [CrossRef]
20. Sivapathasundaram, M.; Mahendran, M. Numerical Studies and Design of Thin Steel Roof Battens Subject to Pull-through Failures. *Eng. Struct.* **2017**, *146*, 54–74. [CrossRef]
21. Sivapathasundaram, M.; Mahendran, M. Pull-out Capacity of Multiple Screw Fastener Connections in Cold-Formed Steel Roof Battens. *J. Constr. Steel. Res.* **2018**, *144*, 40–52. [CrossRef]
22. Lu, Q.; Li, M.; Zhang, M.; Min, Q.; Zhang, Y.; Liu, X. Wind-Resistance Performance Investigation of 360° Vertical Seam-Locked Roof System Reinforced by Sliding Support and Sandwich Panel. *J. Build. Eng.* **2022**, *45*, 103689. [CrossRef]
23. Rocha, D.; Eamon, C.D.; Murphy, J.F. Reliability Analysis of Roof Sheathing Panels Exposed to a Hurricane Wind. *Struct. Saf.* **2011**, *33*, 74–81. [CrossRef]
24. Ji, X.; Huang, G.; Zhang, X.; Kopp, G.A. Vulnerability Analysis of Steel Roofing Cladding: Influence of Wind Directionality. *Eng. Struct.* **2018**, *156*, 587–597. [CrossRef]
25. Huang, G.; Ji, X.; Luo, Y.; Gurley, K.R. Damage Estimation of Roof Panels Considering Wind Loading Correlation. *J. Wind. Eng. Ind. Aerod.* **2016**, *155*, 141–148. [CrossRef]
26. Huang, M.; Ye, H.; Lou, W.; Sun, X.; Ye, J. Wind-induced vibration and fatigue analysis of long span lattice structures considering distribution of wind speed and direction. *J. Zhejiang Univ. (Eng. Sci.)* **2019**, *53*, 1916–1926. (In Chinese)
27. Fan, J.; Guo, X.; Wu, C.; Deng, D. Fast Evaluation of Fatigue Behavior of Q235 Steel by Infrared Thermography and Energy Approach. *J. Mater. Eng.* **2012**, *12*, 71–76. (In Chinese)
28. Miner, M.A. Cumulative Damage in Fatigue. *J. Appl. Mech.* **1945**, *12*, 159–164. [CrossRef]
29. Matsuishi, M.; Endo, T. Fatigue of Metals Subjected to Varying Stress. *J. Soc. Mech. Eng.* **1968**, *68*, 37–40.
30. Li, Q.S.; Hu, S.Y.; Dai, Y.M.; He, Y.C. Field Measurements of Extreme Pressures on a Flat Roof of a Low-Rise Building During Typhoons. *J. Wind. Eng. Ind. Aerod.* **2012**, *111*, 14–29. [CrossRef]
31. Xu, Y.L.; Reardon, G.F. Test of Screw Fastened Profiled Roofing Sheets Subject to Simulated Wind Uplift. *Eng. Struct.* **1993**, *15*, 423–430. [CrossRef]

32. Xu, Y.L.; Teng, J.G. Local Plastic Failure of Light Gauge Steel Roofing Sheets: Finite Element Analysis Versus Experiment. *J. Constr. Steel. Res.* **1994**, *30*, 125–150. [CrossRef]
33. Chen, K.; Shen, J.; Yu, G.; Zhu, W.; Li, W.; Zhang, S. Parameter Determination of Mooney-Rivlin Model and Finite Element Simulation of the Compression Deformation of Rubber Rail Fastener. *Mater. Mech. Eng.* **2016**, *40*, 89–92. (In Chinese)